JOURNAL OF MATERIALS SCIENCE 30 (1995) 481–487

# Determination of fracture stress and strain of highly oriented short fibre-reinforced composites using a fracture mechanics-based iterative finite-element method

K. M. BROCKMÜLLER*
*Kernforschungszentrum Karlsruhe GmbH, Inst. IRS, Postfach 3640, 76021 Karlsruhe, Germany*

O. BERNHARDI†
*BASF AG Ludwigshafen, Dept. KTE/TM, 67056 Ludwigshafen, Germany*

M. MAIER
*Inst. f. Composite Materials Ltd, University of Kaiserslautern, Erwin-Schrödinger Str. 58, 67663 Kaiserslautern, Germany*

For a tensile test specimen made of a short fibre-reinforced composite with the fibres oriented in the direction of force, a model was developed to describe the onset and propagation of microcracks, which finally lead to macroscopic failure of the specimen. The crack propagation theory used is based on a standard fracture mechanics method and was applied to the microstructure of the specimen by the finite element method. The results appear qualitatively correct. The micromechanical method applied gives a deeper insight into the fracture processes within short fibre-reinforced composites.

## 1. Introduction

The failure stress and strain of a short fibre-reinforced composite under continuously increasing tensile load depends on the macroscopic geometrical shape of the body, the introduction of forces into the body, the material properties (which may in turn depend on the rate of stress/strain increase, humidity and temperature), the existence of flaws and micro- or macrocracks as well as the microscopic positioning of the fibres. In this paper, a standard tensile test specimen under a steadily increased external load is considered. It is assumed that all the fibres are oriented in the direction of the external load and that they are periodically placed within the specimen. It is further assumed that there are no flaws such as air inclusions or microcracks.

Tensile test specimens made of short fibre-reinforced composites are usually fabricated by injection techniques. The flow field of the initially molten material leads to a strong orientation of fibres in the injection direction [1, 2], which in the later testing is the direction of applied force. For such specimens, several authors observed the onset of acoustic emission after some initial specimen deformation [3–7]. These acoustic emissions correspond to microfailure events within the specimens. The number of emission signals per unit strain rises approximately exponentially with increasing strain. Since at the lower strains a specimen is deformed uniformly it is reasonable to assume that the failure events are evenly distributed over the volume of the specimen.

This assumption is strengthened by observations of Sato *et al.* [8, 9] who investigated the continuously loaded tensile stressed side of a short glass fibre-reinforced polyamide 66 specimen ($l_f = 0.4$ mm, $d_f = 13$ μm, $V_f = 16\%$) under a scanning electron microscope:

- At low strains, microcracks close to the fibre ends were formed within the matrix. Concurrently, matrix flow was observed near the fibre ends.
- At about 75% of the specimen rupture load the fibre ends lost contact with the matrix and microcracks starting at the fibre ends propagated along the sides of the fibres.
- With a further increase in load, microcracks formed between adjacent fibres and matrix flow was observed near these microcracks.
- Finally the cracks grew together, thus leading to macroscopic failure of the specimen.

Similar observations were made by Choi [3] and Curtis *et al.* [10].

Based on these observations, a microscopic failure model for a short fibre-reinforced specimen should describe the onset and development of microcracks

* *Present address*: Rasna Corporation (Europe), Am Kronberger Hang 2, 65824 Schwalbach-Kronberg, Germany
† *Present address*: Asea Brown Boveri, Corporate Research Center, CRH, Czernyring 22, 69115 Heidelberg, Germany

0022–2461  

distributed over a specimen with increasing load. The final failure in such a model appears when the cracks grow together, dividing the model in half.

Termonia [11] developed a finite difference type model based on several perfectly oriented but randomly distributed fibres of differing lengths in a matrix. In his model the total strain is increased gradually and the kinetic failure theory together with a Monte-Carlo scheme is used to predict the failure of individual "bonds" between nodes. Special consideration is given to the fibre matrix bonding, which was varied in the investigations. The first results presented fit the experimental observations discussed above; further experimental investigation, however, is still necessary.

In this paper the extensions of microscopic cracks are described on the basis of fracture mechanics, not bond strength. Fracture mechanics methods have proved to be reliable for macroscopic bodies with cracks (locations with infinite stresses).

## 2. Description of the model

### 2.1. Finite element (FE) model of an undamaged specimen

In an earlier contribution [12] a 3-dimensional finite element model of a highly oriented short fibre-reinforced composite was described and discussed. This model possessed several properties, the simplest of which was the good predictions it gave of composite stiffness. Since the intended micromechanical fracture description required a finer mesh, this 3D model had to be reduced to two dimensions in order to save nodes and elements, thereby enabling a 2D mesh refinement. We will merely outline the derivation of this 2D model here; for details see [1] or [12].

Fig. 1 shows the assumed relative placement of fibres in the $x$–$z$ plane. In this symmetry it is sufficient to model a unit cell with finite elements, if the symmetry conditions are taken care of with respective boundary conditions at all sides of the model. For a load in the $z$ direction these boundary conditions are:

- Nodes at the bottom ($z = z_{min}$): no displacement allowed in the $z$ direction.
- Nodes at the top ($z = z_{max}$): displacement in the $z$ direction is forced to be the same for all nodes.

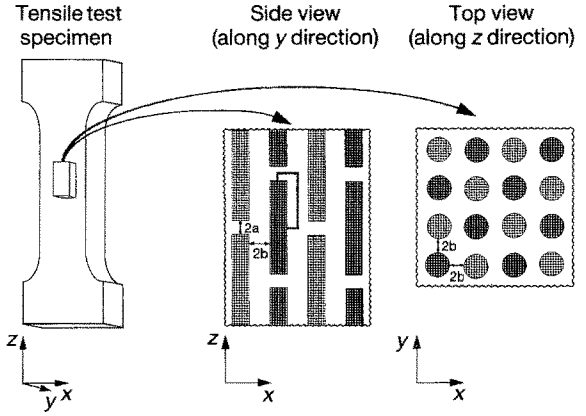


*Figure 1* Assumed relative placement of fibres within a specimen with a high degree of fibre orientation.

- Nodes at the left ($x = x_{min}$): no displacement allowed in the $x$ direction.
- Nodes at the right ($x = x_{max}$): this plane is not an ordinary symmetry plane since the mirror image of the side $x > x_{max}$ at the line $x_{max}$ does not coincide with the side $x < x_{max}$. However, there is a point symmetry for each node having $z = (z_{max} + z_{min})/2$. If one regards any of these nodes the following symmetry relations hold for all nodes with the same value of $x$

$$U_x(I) + U_x(J) = 2 \cdot U_x(K)$$
$$U_z(I) + U_z(J) = 2 \cdot U_z(K)$$

$K$ is the node with $z = (z_{max} + z_{min})/2$. The nodes $I$ and $J$ have the same $x$ value as $K$, but lie symmetrical to $K$ (one above and the other below). The terms $U_x(K)$ and $U_z(K)$ take care of a general displacement of the plane, which is caused by Poisson contraction in the case of $U_x(K)$. The nodes $I$ and $J$ always move anti-symmetrically with respect to $K$.

Apart from these constraints the used symmetry introduces as a free parameter the quotient $a/b$ (see Fig. 1). If everything else is kept fixed, this parameter controls how close the fibres lie together in the $x$ (respectively $y$) and the $z$ directions. A good assumption for its default value is $a/b = 1$ [1, 12].

The FE mesh used is shown in Fig. 2. It was modelled with 4-node quadrilateral elements with $2 \times 2$ integration points (ANSYS program: STIF42). The option for rotational symmetry was used. This has the advantage that the modelled unit cell appears to see rotationally symmetric conditions to its neighbours with respect to the $z$ axis, which is more realistic than assuming a plane strain or plane stress condition. On the other hand, note that it is impossible to fill up a 3D space with adjacent rotationally symmetric unit cells. On the whole the predictions of composite stiffness with this rotationally symmetric model come close to a few percent of those of the above-mentioned 3D model, which in turn was shown to be rather good [1, 12].

Since fibres in real composites do not have a coupling agent at the ends (fibres are broken after being coated) the model assumes no contact (i.e. no load-carrying capability) between fibre end and matrix. This means that a tensile load applied on the composite in the $z$ direction opens a microcrack at the top of the fibre between fibre and matrix. This in turn leads to singular stress behaviour at the fibre end ($x = r_f$, $z = l_f/2$) (which was illustrated in [1, 12]).

### 2.2. Fracture mechanics approach to modelling microcrack propagation

Since stresses are singular at the fibre ends it is assumed that with increased load cracks will start to propagate from these locations. Fig. 3 shows several possible paths. All cracks in this model propagate simultaneously due to the high symmetry of the model. When the cracks grow together the FE model separates into two parts, corresponding to the modelled specimen separating into an infinite number

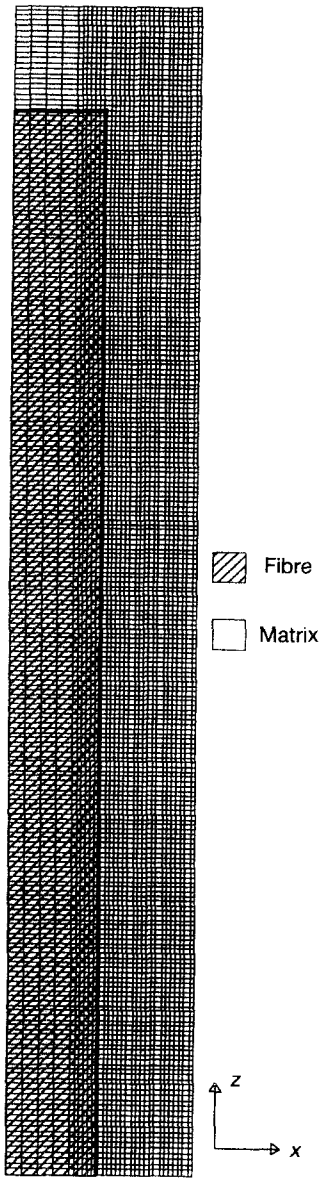


*Figure 2* Typical finite element mesh used in the analysis, consisting of 220 × 30 elements.

of parts. Note that the propagation of identical cracks and the separation into not just two parts stems from the idealization of this model makes with respect to the relative fibre placement.

The stress conditions for crack propagation and the crack paths were determined with the help of a classical fracture mechanics criterion. A well tested criterion for elastic and isotropic materials to determine whether or not a crack will propagate under a given load is Irwin's $G$ criterion of the energy release rate [13, 14]. It is based on the elastic energy $\partial U$ released per additional crack area $\partial A$ of a virtual crack extension under a given load and for a given direction of crack propagation

$$G = -\partial U/\partial A$$

This value is compared with a critical value $G_c$, which depends only on the material through which the crack travels. If $G < G_c$ for a given load the crack will not propagate; otherwise it will. The direction a crack will take in a homogeneous and isotropic medium is that in which the calculated value of $G$ has a maximum [14].

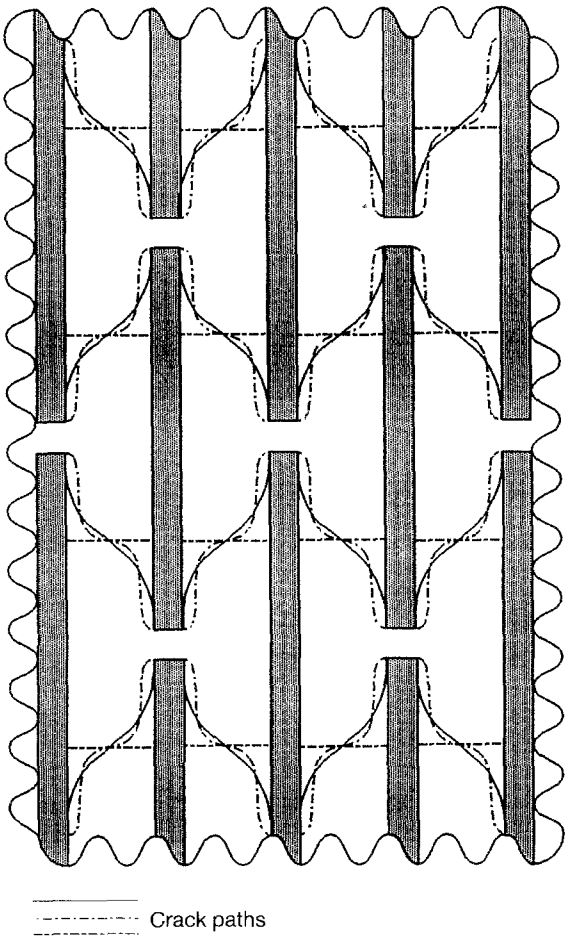


*Figure 3* Considered crack paths: the symmetry of the paths results from the symmetry of the fibre arrangement.

For correct calculation of the crack propagation the following procedure should be carried out. The load on the model should be increased in small steps. Following each increase in load, several FE meshes with small cracks in different directions starting from the existing crack should be generated and the corresponding values of $G$ should be calculated. If any of these values exceeds $G_c$ the crack should be extended by a small amount in the direction corresponding to $G_{max}$, as described above. Before further increasing the load it must be ascertained whether this configuration is stable with respect to the applied load by repeating the virtual crack propagation process until the crack is stable. Should no stable state be reached the crack will (unstably) travel towards another crack coming from the neighbouring unit cell due to the symmetry. When these cracks meet the modelled specimen rips apart.

This procedure requires an algorithm to automatically generate an FE mesh for an arbitrary crack geometry. However, the mesh generator provided by the FE program used did not work reliably so that instead the following simplified procedure was carried out. For the mesh shown in Fig. 2 and the geometrical and material values given in Table I, several possible crack paths as indicated in Fig. 4 were investigated by decoupling adjacent elements by new nodes introduced into the model. First consider the path shown in bold: the crack path was assumed to continue from the pre-existing crack (see above) at the fibre end ($x = r_f$, $z = l_f/2$), since due to the stress singularities this

should be the "weakest" point in the model. This assumption is strengthened by the experimental observations described in the introduction. This crack was elongated in successive calculations in the negative (downward) $z$ direction along the fibre matrix interface and, from a certain point on, in successive calculations in the positive (to the right) $x$ direction through the matrix until it reached the border of the model. All FE calculations were performed at a total model strain of $\varepsilon = 1\%$. For each case the potential energy in the model $U(\varepsilon = 1\%)$ was calculated, so that $G$ as defined above could be evaluated from successive calculations, assuming materially linear behaviour.

TABLE I Default geometrical and material parameters used in the investigations.

| Parameter | Value |
|---|---|
| $r_f$ | 7 μm |
| $l_f$ | 0.18 mm |
| $V_f$ | 17.58% |
| $E_f$ | 70000 N mm$^{-2}$ |
| $\nu_f$ | 0.35 |
| $E_m$ | 1990 N mm$^{-2}$ |
| $\nu_m$ | 0.42 |
| $G_{c,fibre-matrix}$ | 0.0309 kJ m$^{-2}$ |
| $G_{c,matrix}$ | 0.0483 kJ m$^{-2}$ |

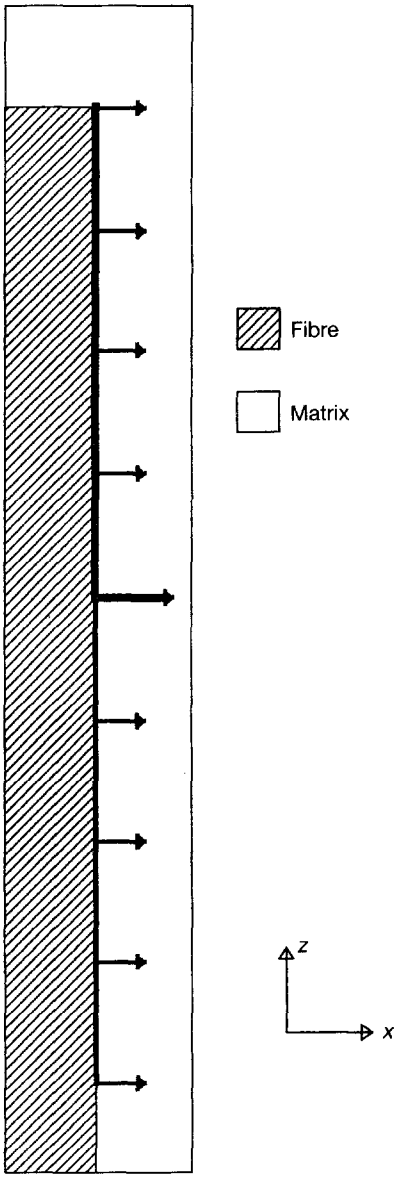


*Figure 4* Crack paths investigated.

The bold curve in Fig. 5 shows the behaviour of $G$ with increasing fracture area $A$. As shown above, $G$ scales proportionally with the potential energy $U$ which implies that $G$ is quadratic in the applied external strain $\varepsilon$. The $G$ values shown in Fig. 5 therefore scale with $\varepsilon^2$. When the strain is continuously increased starting from $\varepsilon = 0\%$ then, at a certain strain, $G$ will exceed $G_{c,fibre-matrix}$ and the crack will open up to the respective crack area $A$. A further increase in strain will scale the $G$–$A$ curve to higher $G$ values, so that the crack opens further. In this way, stable crack growth with increasing strain will continue up to the crack area $A = 0.00194\ mm^2$. Assume for the time being that the crack will now propagate into the matrix. This leads to a change in stress mode at the crack tip, which explains the sudden increase in $G$. From then on, the calculated $G$ must be compared with $G_{c,matrix}$ as opposed to $G_{c,fibre-matrix}$. The falling of the $G$–$A$ curve again means stable crack growth with increasing total strain. At the strain corresponding to the following minimum in $G$, however, the crack becomes unstable: this means that without a further increase in externally applied strain the crack growth releases more potential energy from the model than is needed to drive the crack further, thereby leading to failure of the whole model.

Fig. 4 also shows several other cracks. Their paths merely differ from the crack described above in the amount of cracking allowed in the $z$ direction, before turning off in right angles into the matrix. The corresponding $G$ versus $A$ dependencies are also shown in Fig. 5. We must now discuss which of these cracks comes closest to reality. Tensile tests with short fibre-reinforced specimens have a continuously increasing stress–strain curve until suddenly the specimen fails. This implies that the final failure of the specimen is through cracks growing together unstably. Looking at the investigated cracks in Fig. 5 starting from the left, the crack corresponding to the bold line is the first to fulfil this criterion. It may be noted further that the instability is more significant in the bold curve than in all others. The reason for this lies in the fact that due

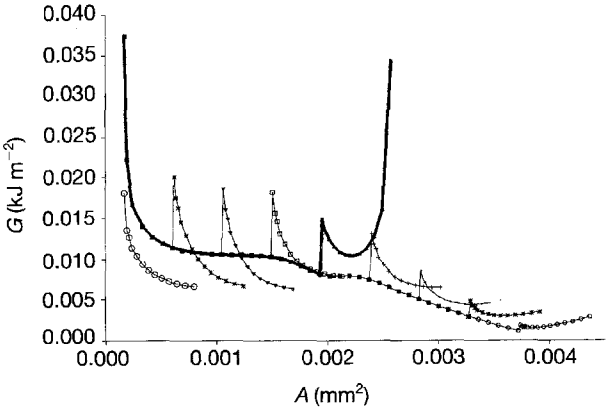


*Figure 5* Dependence of the energy release rate $G$ on the total crack area $A$ at a model strain of 1% for several crack paths.

to the chosen geometry only this crack grows frontally towards a crack in the neighbouring cell simulated by the boundary conditions. It is therefore reasonable to consider the crack drawn in bold in Fig. 4 as the crack "closest to reality". In the further discussion only this crack path will be considered.

## 2.3. Derivation of stress–strain curve from $G$–$A$ dependence

We will now derive from the $G$ versus $A$ dependence an $\varepsilon$ versus $A$ dependence. In Fig. 5 all $G$ values were calculated for $\varepsilon = 1\%$. As explained earlier $G$ scales quadratically with $\varepsilon$. To determine at which strain $\varepsilon$ a failure from crack area $A$ to $A + \Delta A$ will develop the following scaling formula can be used

$$\varepsilon(A) = \sqrt{\frac{G_c}{G(A,\varepsilon = 1\%)}} \cdot 1\%$$

Here $G_c$ must be set to $G_{c,\text{fibre-matrix}}$ or to $G_{c,\text{matrix}}$ according to whether the crack travels along the fibre/matrix interface or through the neat matrix.

The corresponding FE model with the respective crack has a stiffness $E(A)$ depending on the crack area. Therefore the overall model stress $\sigma$ corresponding to the strain $\varepsilon$ can be calculated via $\sigma(A) = E(A) \cdot \varepsilon(A)$.

Using the assumptions $G_{c,\text{fibre-matrix}} = 0.0309\ \text{kJ m}^{-2}$ and $G_{c,\text{matrix}} = 0.0483\ \text{kJ m}^{-2}$, the derivation of which is discussed in the next section, one obtains the stress–strain curve shown in Fig. 6. The dots represent $\sigma$–$\varepsilon$ pairs for consequent cracks. Consider the specimen being exerted to steadily increasing external strain. The crack grows along the fibre–matrix border (open points) up to a strain of about 2% where it angles off into the matrix (filled points) until the crack becomes completely unstable at $\varepsilon = 2.16\%$. Note that the indicated retraction of the strain when the crack changes its direction is due to the evaluation method and is not physical. The fact that the specimen does not rip apart at the calculated point of maximum stress but at higher strains is probably due to the simplified assumption made about the crack path.

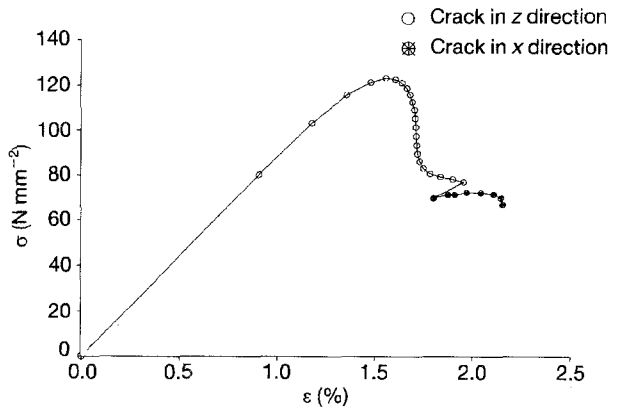


*Figure 6* Stress–strain behaviour resulting from the assumed growing of cracks.

## 2.4. Determination of $G_c$ values

The values for $G_c$ used above were determined by a comparison of an experiment with the corresponding FE calculations for a specimen with the same geometrical and material data. It was assumed that the experimentally observed maximum stress corresponds to a state in which the crack is still between fibre and matrix, while the experimentally observed failure stress corresponds to the unstable formation of the matrix crack. These assumptions are motivated by the stress–strain behaviour shown in Fig. 6.

The $G_{c,\text{matrix}}$ value used in the previous section to derive the stress–strain curve is roughly two orders of magnitude lower than those quoted in the literature [15]. This discrepancy may be due to the fact that the macroscopic measurement is carried out on a specimen made of neat matrix whereas in this case the fibres restrict matrix deformation and lead to different failure modes. This discrepancy is discussed in detail in [1].

# 3. Results

## 3.1. Dependence of failure stress and strain on geometrical and material parameters

The technique described above was used to study the dependence of failure stress and strain on individual model parameters, namely the fibre length $l_f$, fibre radius $r_f$, fibre volume fraction $V_f$ and fibre modulus $E_f$. The results are shown in Figs 7–10. Each of these curves is based on a standard model composite with properties according to Table I where only the investigated parameter was varied.

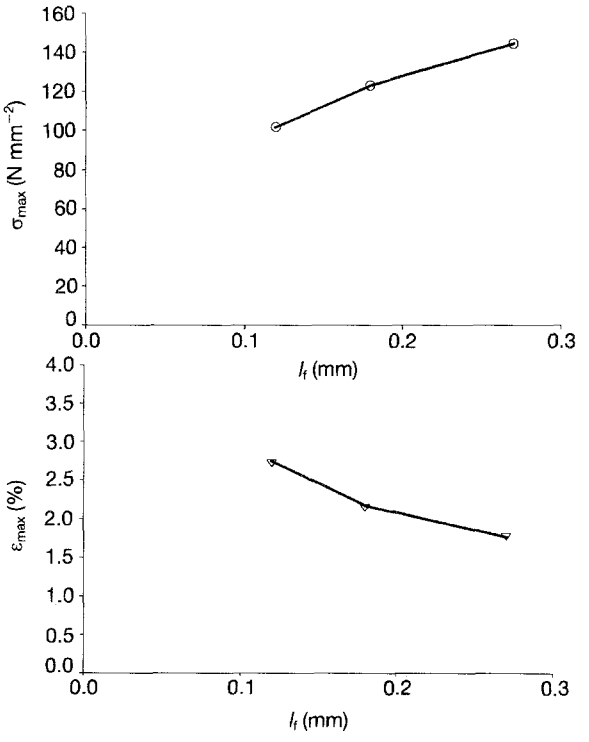


*Figure 7* Influence of the fibre length $l_f$ on composite maximum stress $\sigma_{max}$ and strain $\varepsilon_{max}$.

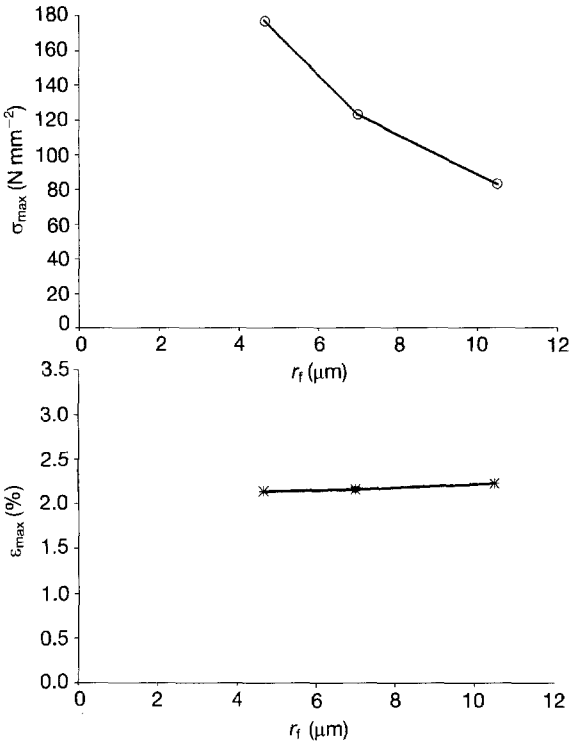


*Figure 8* Influence of the fibre radius $r_f$ on composite maximum stress $\sigma_{max}$ and strain $\varepsilon_{max}$.

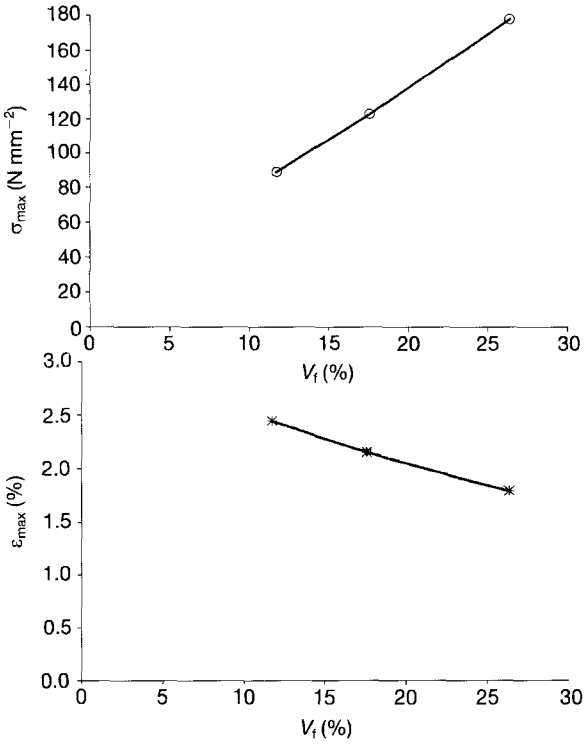


*Figure 9* Influence of the fibre volume $V_f$ on composite maximum stress $\sigma_{max}$ and strain $\varepsilon_{max}$.

In order to qualify the model described here a comparison between experimental observations and model predictions had to be made.

### 3.2. Qualitative comparison of predictions with results of other experimenters

This comparison was made on a qualitative rather than quantitative basis since in all the experiments

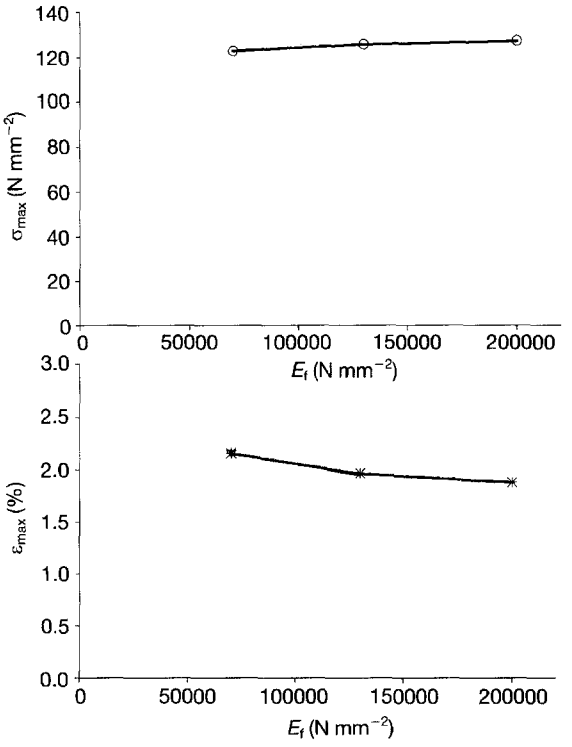


*Figure 10* Influence of the fibre modulus $E_f$ on composite maximum stress $\sigma_{max}$ and strain $\varepsilon_{max}$.

cited in the literature some data were missing, precluding the possibility of a precise evaluation by this model. The following experimental observations on highly orientated short fibre-reinforced specimens by Ramsteiner and Theysohn [16] and Curtis *et al.* [10] are, however, qualitatively predicted by the model introduced here:

(i) failure stress increases with increasing fibre volume fraction $V_f$ [10, 16];
(ii) failure strain decreases with increasing fibre volume fraction $V_f$ [10];
(iii) failure strain decreases with increasing fibre length $l_f$ [10] and
(iv) failure strain decreases with increasing fibre modulus $E_f$ [10].

## 4. Conclusions

For the special case of highly oriented short fibres in a matrix under load in the fibre direction a combination of FE model with a standard fracture mechanics concept was developed to predict the failure stress and strain of a composite for which all geometrical and material parameters ($l_f$, $d_f$, $V_f$, $E_f$, $E_m$, $v_f$, $v_m$, $G_{c,fibre-matrix}$, $G_{c,matrix}$) may be chosen freely. The model makes rather crude assumptions about the ideal structure of the composite and about the crack path. This leads to a stress–strain curve for continuously increased loading which does not describe experimental observations on real specimens too well for large strains. However, the microcracking at small strains which is also observed in acoustic emission analyses is predicted. Further, the failure stresses and strains correlate well qualitatively with experimental observations.

The model presented here should not be thought of as being fully developed. However, the investigations presented here should encourage further research in the direction of FE algorithms combined with fracture mechanics for predicting composite failure behaviour.

For completeness, it should be noted that an extension of this model for the case of a macroscopic interlayer between fibres and matrix has also been developed. This is documented in [1].

## Acknowledgements

K. Brockmüller is grateful for support from the BASF AG Ludwigshafen, Departments ZKV/F and ZXT for financial support, and valuable discussions with numerous colleagues, especially from department KTE/TM.

## References

1. K. BROCKMÜLLER, "Zur Vorhersage des Spannungs-Dehnungs-Verhaltens kurzfaserverstärkter Verbundwerkstoffe mittels der Methode der Finiten Elemente", Dissertation D 386, Universität Kaiserslautern (1992).
2. F. RAMSTEINER and R. THEYSOHN, *Composites* **10** (1979) 111.
3. N. S. CHOI, "Acoustic emission and micromechanistic failure processes in short glass fibre reinforced poly(ethylene terephthalate)", Dissertation, Interdisciplinary Graduate School of Engineering Sciences, Kyushu University, Fukuoka, Japan (1990).
4. N. SATO, T. KARAUCHI, S. SATO and O. KAMIGAITO, *J. Mater. Sci.* **19** (1984) 1145.
5. N. SATO, T. KARAUCHI, S. SATO and O. KAMIGAITO, *J. Composite Mater.* **22** (1988) 850.
6. N.-S. CHOI and K. TAKAHASHI, *ibid.* **24** (1990) 1012.
7. J. BOHSE, G. KROH and H. WOLF, *Kunststoffe* **81** (1991) 543.
8. N. SATO, T. KARAUCHI, S. SATO and O. KAMIGAITO, "In situ SEM observation of fracture processes in short glass fibre reinforced thermoplastic composite", *Special Technical Publication* 868 (ASTM, Philadelphia, 1985) p. 493.
9. N. SATO, T. KARAUCHI, S. SATO and O. KAMIGAITO, *J. Mater. Sci.* **26** (1991) 3891.
10. P. T. CURTIS, M. G. BADER and J. E. BAILEY, *ibid.* **13** (1978) 377.
11. Y. TERMONIA, *ibid.* **25** (1990) 4644.
12. K. M. BROCKMÜLLER and K. FRIEDRICH, *ibid.* **27** (1992) 6506.
13. G. R. IRWIN, "Fracture", in "Handbuch der Physik", Band VI, edited by S. Flugge (Berlin, 1958) p. 551.
14. H.-A. RICHARD, "Bruchvorhersagen bei überlagerter Normal- und Schubbeanspruchung von Rissen" (VDI Forschungsheft, VDI-Verlag, Düsseldorf, **631/85**, 1985).
15. H.-H. KAUSCH, "Polymer fracture", Polymers/properties and applications series (Springer-Verlag, Berlin, 1987), 247 ff. and 312.
16. F. RAMSTEINER and R. THEYSOHN, *Compos. Sci. Technol.* **24** (1985) 231.

*Received 11 June 1993*
*and accepted 9 June 1994*